HHS Public Access

Author manuscript

J Phys Chem Lett. Author manuscript; available in PMC 2024 June 06.

Published in final edited form as:

J Phys Chem Lett. 2024 February 29; 15(8): 2270–2278. doi:10.1021/acs.jpclett.3c02589.

Predicted and Experimental NMR Chemical Shifts at Variable Temperatures: The Effect of Protein Conformational Dynamics

Xu Yi[#],

Lichirui Zhang[#],

Richard A. Friesner,

Ann McDermott

Department of Chemistry, Columbia University, New York, New York 10025, United States

Abstract

NMR chemical shifts provide a sensitive probe of protein structure and dynamics but remain challenging to predict and interpret. We examine the effect of protein conformational distributions on ^{15}N chemical shifts for dihydrofolate reductase (DHFR), comparing QM/MM predicted shifts with experimental shifts in solution as well as frozen distributions. Representative snapshots from MD trajectories exhibit variation in predicted ^{15}N chemical shifts of up to 25 ppm. The average over the fluctuations is in significantly better agreement with room temperature solution experimental values than the prediction for any single optimal conformations. Meanwhile, solid-state NMR (SSNMR) measurements of frozen solutions at 105 K exhibit broad lines whose widths agree well with the widths of distributions of predicted shifts for samples from the trajectory. The backbone torsion angle ψ_{i-1} varies over 60° on the picosecond time scale, compensated by φ_i. These fluctuations can explain much of the shift variation.

Graphical Abstract

Corresponding Author Ann McDermott – Department of Chemistry, Columbia University, New York, New York 10025, United States.

[#]Author Contributions

X.Y. and L.Z. made comparable contributions.

Supporting Information

The Supporting Information is available free of charge at https://pubs.acs.org/doi/10.1021/acs.jpclett.3c02589.

Experimental details of sample preparation and spectra collection, detailed description of molecular dynamics simulations and computational calculation, protein secondary diagram, the RMSD changes in molecular dynamics simulations, correlations between experimental and computational chemical shifts and torsion angles, correlations between torsion angles, N—C correlation spectra, chemical shifts and solvent exposure among snapshots extracted from molecular dynamics simulations, structures of the two representative conformations captured in molecular dynamics simulations, RMSD of all the backbone heavy atoms (PDF)

The authors declare no competing financial interest.

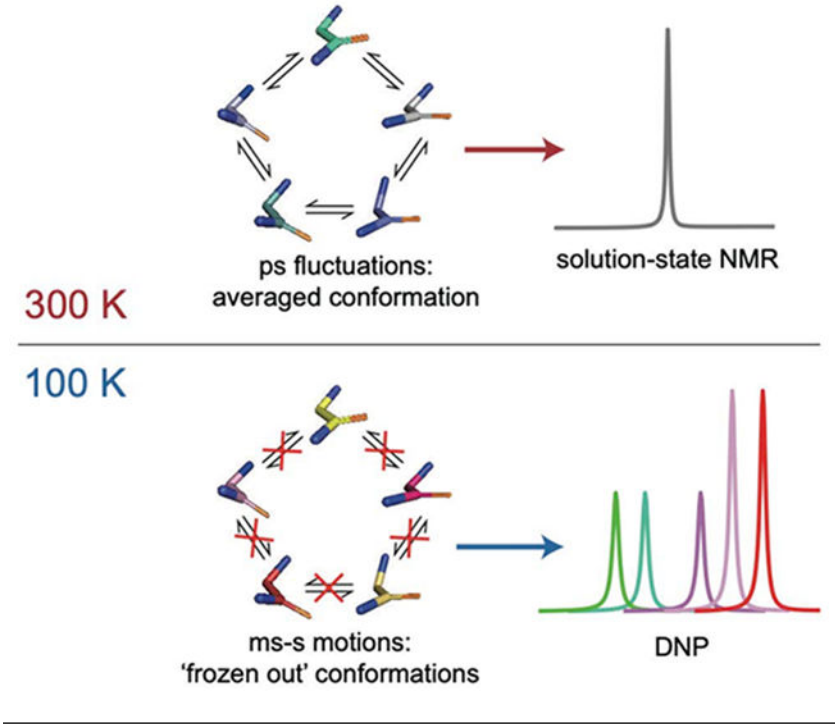

1. INTRODUCTION

NMR chemical shifts provide a sensitive probe of protein structure and dynamics.[1-3] For example, prior studies indicate that ^{15}N chemical shifts are strongly influenced by local protein structure,[1,4,5] including backbone torsion angles[6,7] as well as electrostatic or hydrogen bonding effects. Accurate ab initio prediction shifts would assist in interpretations of experimental data, but important challenges remain, including the frequently measured amidic ^{15}N sites.

A number of studies suggest that conformational averaging contributes to the complexity of shift interpretation.[8-10] With hybrid quantum mechanics/molecular mechanics/molecular dynamics (MD-QM/MM), improved accuracy of calculations of ^{15}N chemical shift tensors has been reported.[11] Strong support for the importance of conformational averaging comes from cryogenic solid-state NMR (SSNMR) studies of proteins for which significant NMR line broadening has been observed,[12-18] consistent with freezing out disparate members of the ensemble. Other studies support the hypothesis that broad line widths in low temperature NMR are due to static conformational heterogeneity[14-18] including direct measurements of distribution in the local torsion angles.[19] This points to the possibility of characterizing the protein conformational ensemble using low temperature NMR line widths.

In this study, we demonstrate the impact of conformational ensembles on NMR shifts, focusing on the antibiotic target, dihydrofolate reductase (DHFR), which has been well studied in terms of NMR chemical shifts and conformational dynamics. We focus on a specific site for which abundant experimental data are available, and which is evidently stably folded in a β strand conformation, I60. As is shown in Figure S1, I60 is located in

the middle of β-sheet C (residues 58–63) and tends to form hydrogen bond interaction with adjacent β-sheet B (residues 39–43) and β-sheet D (residues 73–75). *E. coli* DHFR protein (UniProt: P0ABQ4) was expressed in M9 minimal media supplemented with combinations of corresponding isotopic enriched amino acids. The purified protein was saturated with trimethoprim (TMP) which is a well-known inhibitor of DHFR. The protein sample was prepared as described in Materials and Methods section in Supporting Information before taking NMR experiments. Given that the observation of broad backbone amide ^{15}N NMR line widths at low temperature is relatively general, we also make comparisons with other sites.

2. RESULTS

2.1. QM/MM Calculation Based on MD Simulation.

For protein systems, hybrid quantum mechanics/molecular mechanics (QM/MM) has been applied with success previously. This approach results in increasingly reasonable computational demands, showing excellent and improving accuracy.[20] Here the QM/MM approach was implemented with an automated fragmentation (AF) procedure, which was previously benchmarked with 20 proteins.[21]

To investigate the importance of conformational sampling in NMR shifts, we computed an MD trajectory and selected samples from it to prepare an appropriate ensemble of native and near native conformations. This group of conformations was then studied using QM/MM to predict chemical shifts. A 1000 ns MD simulation was performed based on a solved DHFR:TMP X-ray crystal structure.[22] The backbone heavy atoms root mean square deviation (RMSD) referenced to the initial state is shown in Figure S2a, demonstrating the overall stability of the whole protein during the MD trajectory. QM/MM calculations were used to study chemical shifts for snapshots extracted from the MD simulation. To study the effects of solvent, the locations and orientations of water molecules from the MD simulation were imported to AF-QM/ MM. A DHFR:TMP X-ray crystal structure[22] with a resolution of 2.5 Å and *R*-value of 0.23 was used for direct QM/MM calculation and MD simulation. Details of the MD simulation protocols and QM/MM calculation of the coordinates of each MD snapshot and X-ray crystal structure are presented in the Materials and Methods section in Supporting Information.

To represent solution-state NMR data, the predicted shifts were averaged over the ensemble. Figure S3 shows the comparison between the chemical shift prediction from the X-ray crystal structure[22] and that averaged over the conformations sampled with MD. Both the X-ray crystal structure and the MD snapshots were energy minimized before QM/MM calculations. The correlation coefficient comparing experimental solution ^{15}N shifts to single conformer (X-ray crystal structure) predicted shifts is 0.69 and for $^{13}C\alpha$ is 0.78. We then extracted 20 snapshots from the 1000 ns MD simulation, regularly sampled with an interval between snapshots of 50 ns. QM/MM calculations for each of the 20 snapshots using AF-QM/MM resulted in predicted average chemical shift with a better correlation to experimental solution-state NMR shifts, 0.73 for ^{15}N and 0.94 for $^{13}C\alpha$. By another metric, the root mean square error (RMSE) (RMSE = $\sqrt{\frac{\sum_{i=1}^{N} | y(i) - \hat{y}(i) |^2}{N}}$, where N is the

number of data points, $y(i)$ is the i-th measurement, and $\hat{y}(i)$ is its corresponding prediction) can be thought of as a prediction accuracy and was 4.8 ppm (^{15}N) and 1.7 ppm ($^{13}C\alpha$), respectively, when averaging was included, vs 7.9 and 3.6 ppm for the corresponding single conformation predictions. $^{13}C'$ QM/MM calculation results do not match the experimental chemical shift assignments as well as $^{13}C\alpha$ (correlation coefficient $r = 0.51$, RMSE = 2.3 ppm). Possibly the large chemical shift anisotropy (CSA) of the carbonyl, the resonance effects, and the important effects of hydrogen bonds are not well captured in the MD sampling. The improvement in the ^{15}N shift prediction accuracy due to averaging is significant, especially given the importance of ^{15}N shift measurements in protein studies.

The shift prediction is relatively stable over the trajectory. Averaging snapshots from the different time ranges of the MD trajectory gives a similar chemical shift correlation with experimental results (Figure S4). The correlation is similar when extracting the snapshots from the first 200 ns, the last 200 ns, or the middle 200 ns in MD simulation. This result indicates that the whole MD calculation is stable, and the improvement due to hybrid QM/MM calculations and MD simulation is reproducible. Moreover, the key fluctuations that contribute to chemical shift averaging appear to operate on a relatively fast time scale consistent with the hypothesis that these fluctuations are averaged in the fast limit in solution NMR measurements.

In contrast with the narrow NMR spectra at room temperature, protein NMR peaks at low temperature are notably broad, putatively because various conformations freeze to create an inhomogeneous mixture. Since the QM/MM predicted shifts averaged over the MD simulation predict the solution-state NMR chemical shift at room temperature with good accuracy, we asked whether the ensemble of snapshots in the trajectory might be a good representation of the low temperature experimental ensemble. In order to address this question, we compared the amide ^{15}N and ^{13}C chemical shifts of each residue from MD snapshots with spectra collected at cryogenic temperatures. In Figure 1a, the distribution of calculated ^{15}N and ^{13}C isotropic shifts in the snapshots matches well with the experimental contour at 105 K in solid-state NMR (SSNMR). Both the ^{13}C chemical shift range and ^{15}N shift range agree well, comparing the peak pattern and the QM/MM scatter points distribution. For the prediction of the five sites (highlighted in Figure 1c) of IG-DHFR, 85% of the scatter points lay within the contours of DNP spectra (Figure 1b). The chemical shifts were calculated with restricted minimization before QM/MM; without minimization, the predictions are less similar to the low temperature SSNMR experiments, as shown in Figure S5 where the ^{15}N, $^{13}C'$, and $^{13}C\alpha$ shifts are uniformly distributed in the ranges 95–140, 165–185, and 53–68 ppm, respectively. The observation suggests that local minimization applied on MD snapshots before QM/MM allowing an adjustment with heavy atom RMSD < 0.3 ψ is a reasonable simple model for experimental annealing/cooling of the sample.

2.2. Torsion Angle Variation in MD.

The MD sampling studies described above suggest that NMR shifts fluctuate on a fast time scale at room temperature and are frozen into a broad inhomogeneous static distribution at cryogenic temperatures. The question arises as to the origins of these fluctuations in terms of conformational degrees of freedom. Inspecting the snapshots extracted every 10 ns from

the MD trajectory, the torsion angles ψ and φ exhibit wide variations for many residues, as is shown in Figure 2c, Figure S6a,b, and Figure S7a. We focus on Ile60-Ile61 which is located in the middle of a sheet structure in *E. coli* DHFR, Figure 2b. The Ile60 ψ value is 118° based on the X-ray crystal structure of *E. coli* DHFR:TMP,[22] and X-ray crystal structures of *E. coli* DHFR complexes[23] in its catalytic cycle show variation for I60 ψ in a range from 118° to 130°, indicating it as a relatively rigid site with small structural variation among different functional states. Although the ψ angle varies widely in the MD trajectory, Ile60 and Ile61 preserve β-sheet structures throughout the trajectory, and the protein remains locally folded. The scatter points in Figure S8 represent the $\varphi-\psi$ correlation of these two residues in the Ramachandran plot. Such large fluctuations in backbone torison angles are consistent with stably folded structures if the change in one torsion angle is compensated by another, to keep the flanking reisues in the same position. Although ψ and φ both vary by 50° in one amide, for example, Ile60-Ile61 (Figure 2c), the overall volume occupied by the protein chain is not much altered with these variations because of the correlation between ψ_i and φ_{i+1}, which together result in the amide plane "rocking in place" (Figure 2b). Comparing the RMSD of atoms in residue Ile60 Cα vs Ile60O (Figure S9b,c), Ile60Cα ($\overline{\mathrm{RMSD}_{\mathrm{I60C}\alpha}} = 0.38$) is more stationary, while the O atom makes somewhat wider excursions ($\overline{\mathrm{RMSD}_{\mathrm{I60O}}} = 0.48$). A strong correlation between ψ_i and φ_{i+1} is observed also for several other solvent inaccessible residues, Figure S10 and Figure S7a, though some flexible solvent accessible residues showed more complex backbone dynamics. Similar observations in peptide[24-26] and protein[27,28] structures have been previously reported, where a dominant "crankshaft-like" motions in the plane of the amide results in a strong anticorrelated motion between φ_{i+1} and ψ_i. It is noteworthy that other torsion angles such as the side chain torsion angle $\chi 1_i$ also exhibit a variation up to 40° (Figure S6c) do not correlate strongly with backbone torsion angles. The ω_i angle variation in the MD simulation within one amide is ~7°, relatively small compared with other torsion angles, shown in Figure S6d.

2.3. Correlation between N Isotropic Chemical Shifts and Torsion Angles.

Numerous physical effects or structural features such as torsion angles are expected to influence ^{15}N chemical shifts. We specifically focused on the implications of the fluctuation of ψ_{i} on the $\mathrm{N_{i+1}}$ chemical shift for Ile60-Ile61 in *E. coli* DHFR (Figure 3a). This was partly motivated by the broad range of values for ψ observed in the MD simulations. Also, previous low temperature DNP-enhanced NMR experimental data show a correlation between this torsion angle and ^{15}N shifts.[29] A strong correlation between the I61 ^{15}N chemical shifts and I60 ψ values is observed from 100 snapshots in the 1000 ns MD trajectory (Figure 3a). More importantly, both the isotropic chemical shifts and the torsion angles from MD/QM/MM agree with the experimental data. These data support the suggestion that variations in backbone torsion angles within the β basin can have strong effects on the ^{15}N chemical shifts.

The observation of wide variation in both the torsion angle and the ^{15}N shift is not unique for Ile60-Ile61; as shown in Figure S11, most residues also exhibit a broad torsion angle variation of 40° or greater. Most residues also show predicted ^{15}N shift variation over 10 ppm, consistent with the broad lines observed for all residues in low temperature NMR. The correlation of ψ with ^{15}N chemical shifts is apparent for many other residues, as shown in

Figure S11d-f, although it is not evident for every residue (Figure S11a-c). It is likely that the correlation is apparent for Ile60-Ile61 because of the particularly broad range in ψ values sampled by Ile60. The effect of ψ on Ile61 ^{15}N shift is most evident for conformers where the backbone makes excursions out of the most populated sheet basin around ψ = 120° to conformations with ψ > 130°. Typical sheet/strand residues with ψ of 100°−130° show ^{15}N shifts of 127 ±6 ppm. By contrast, sheets that are closer to flat extended conformations with ψ > 150° exhibit shifts of 115 ± 5 ppm (Figure 3a). β strand residues with more restricted ranges of torsion angle ψ from 90° to 130°, such Y111, do not show a significant correlation between backbone torsion ψ and ^{15}N shift and show a narrower span of both ψ and ^{15}N shift (Figure S11a). A master plot QM/MM calculated ^{15}N shifts of all the residues from 100 snapshots with their associated torsion angle ψ (Figure S12) shows that for β sheets the effect of ψ on ^{15}N chemical shifts is most pronounced for ψ 130°−170°, while for sheets with 90°−130°, the dependence is shallow and not monotonic. Ile60-Ile61 is located close to the cofactor binding site, which is empty in the structure that we studied. Possibly the particularly high flexibility of Ile60 is because of this “cavity.” Analogously, the well populated basin for helices (ψ range −50° to 0°) has a mean ^{15}N shift of 116 ± 5 ppm. Helical residues, including Phe31 and Lys109 (Figure S11b,c), have a relatively flat value for the ^{15}N shift as a function of ψ with poorer correlation and a narrower span of both ψ and ^{15}N shift.

Deviation in ^{15}N chemical shifts within a defined range of ψ are as large as 10 ppm, indicating that other structural degrees of freedom besides ψ also contribute to variation in shift. The side chain torsion χ1 has been discussed in relation to influencing backbone chemical shifts and therefore was also examined for correlations with ^{15}N and ^{13}C.[1,30,31] We identified conformations from the MD trajectory with ψ (120° < I60 ψ < 125° in Figure 3b, 150° < 160 ψ < 155° in Figure S13b, 135° < I60 ψ < 140° in Figure S13c). Within each group, ^{15}N chemical shifts vary by more than 3 ppm and side chain torsion angles I60 χ1 vary by up to 30° while staying within the typically preferred “gauche” basin. The correlation plot suggests that χ1 is another factor influencing ^{15}N shifts. The situation is more complex for solvent exposed and flexible residues, such as His149 (Figure S14), which show very broad ranges in torsion angles (including ψ_{i-1} and φ_i) that are not as well compensated by other backbone angles. Consequently, they exhibit broad ranges of $^{15}N_i$ shifts that are not evidently correlated to any one torsion angle (with a span of 25 ppm).

We explored whether the effect of ψ on the ^{15}N shifts might occur because of changes in hydrogen bonding. Variation of backbone torsion angles and rocking of the amide plane described above is expected to modulate the interactions with hydrogen bond partners. This variation is of interest and is expected to have implications for energetics particularly dielectric and electrostatic characteristics. The hydrogen bond between the backbone N—H and neighboring groups, as well as the hydrogen bond between the C—O and other neighboring groups is also expected to affect ^{15}N and ^{13}C′ chemical shifts; both ^{15}N and ^{13}C′ chemical shift tensors are sensitive to the hydrogen bond variations (Figure S15d-f), especially for ^{13}C′ atoms, consistent with previous literature.[32-34] We investigated the hydrogen bond distance and angle over typical snapshots from the 1000 ns MD trajectory. For desolvated residues, such as Ile60-Ile61 in the middle of a sheet structure (Figure 2b), the identity of the protein residues that serve as hydrogen bond partners remains constant,

and the pairwise trajectory was analyzed in terms of the distance and angle of the hydrogen bond. The shortest (or only) hydrogen bond partner for Ile60O is Met42 ^{N}H. This distance varies by 0.6 Å over the trajectory. The shortest (or only) H bond partner of Ile61^{N}H is the carbonyl O of Thr73. The correlation between the Ile61N chemical shifts and Ile60O---H distance, shown in Figure S15a,b, is not strong, though the hydrogen bond angle θ (relative to the C—O vector of I60) shows a strong correlation with the torsion angle ψ. Analysis of solvent-accessible residues is complex because more than one water molecule is normally located within 4 Å of the amide atoms. Overall, it is likely that the strong variation in hydrogen bonding environment is a major reason that ψ influences the ^{15}N shift.

2.4. Time Scale Analysis of Backbone Torsion Angle Dynamics.

In order to assess the time scale of backbone fluctuations, we analyzed a 100 ps segment of the MD simulation with snapshots extracted every 100 fs. The variation of torsion angles for Ile60 ψ is shown in Figure S16a. The angle ranges from 90° to 150°, which is similar to the range observed in the longer time MD simulation shown in Figure 2d. Two states were defined based on the torsion angle range, State 0 with Ile60 ψ < 125° and State 1 with Ile60 ψ > 125°. The structure of Ile60-Ile61 amide undergoes a dynamic and structural change at ~50 ps; before this time, State 0 (Figure S16b) was preferable with Ile60 ψ smaller than 125°, and after that time, State 1 (Figure S16c) with larger ψ was much more favored. Thus, Ile60 ψ is considered as switching between two states, shown in Figure 4a. The time scale of this exchange motion is then determined from the time when Ile60 ψ stays in either state continuously. In the first 50 ps, State 0 occupied more time with a residence time of 0.89 ± 0.18 ps (Figure 4d), while the residence time of State 1 is 0.34 ± 0.05 ps (Figure 4b). In the second 50 ps, the residence time is 0.23 ± 0.02 ps (Figure 4e) for State 0. State 1 is more preferable, and its residence time is longer than what can be extracted from this MD simulation (Figure 4c). This dynamic time scale agrees with previous research about polypeptides,[24] in which the anticorrelated motion of ψ_i and φ_{i+1} is reported to be on the time scale of 0.1 ps. This time scale was associated with protein backbone motions and intermolecular vibrations of the water hydrogen bond network,[35] and these fast time scale atomic fluctuations were observed to facilitate large-scale, slower motions during enzyme catalysis.[36]

The conformational variation of Ile60-Ile61 is likely to be influenced by its partner Thr73, whose O forms a hydrogen bond with Ile61^{N}H. Thr73 is located in another β-sheet structure and is partially solvated, flips conformations at 50 ps, and probably causes the change in its partner Ile60. Thr73 in turn might be affected by the solvent. It forms closest hydrogen bonds with protein residues (Thr73O---Ile61^{N}H, Thr73^{N}H---Asn59O), yet there are also typically water molecules within 3.5 Å of this residue (Figure S16b,c). Because the β-sheet is solvent-exposed, neighboring Trp74O and Val72O both form the shortest hydrogen bonds with water molecules. It is likely that the solvent interactions lead to increased structural variation in Thr73, which then causes it to influence nearby desolvated residues such as Ile60-Ile61 through hydrogen bonding interactions. Longer MD simulations (Figure S6) indicate that the two-state flipping happens regularly and reversibly throughout the trajectory.

3. DISCUSSION

In summary, for relatively buried and structured residues in globular proteins, picosecond time scale large angle fluctuations in backbone torsion angles leads to large dynamic variation in backbone shifts. The changes, despite being over 60° in amplitude, can be consistent with stably folded structures because they are compensated by other torsion angles, and the structure remains in the β basin. The fluctuations should be considered when predicting room temperature shifts. They also contribute significantly to the inhomogeneous low temperature line widths, because the conformations appear to be static (or interconvert very slowly) at 105 K.

The large variation of torsion angles we observed in the MD trajectory may be surprising. Based on our analysis of MD snapshots, it is likely that the compensations from other backbone torsion angles and hydrogen bond angles preserve the global protein secondary structures. Analogous large-amplitude backbone motions have been discussed previously in peptides,[24,37] polymers,[38] and proteins[39,40] with MD simulation in explicit or implicit solvent. In recent research of protein dynamics,[41] several high resolution protein structures were chosen for analyzing the amplitudes of protein motions; the (φ, ψ) distribution of Lys83 captured during dynamics of mouse protein kinase A is up to 150°, and the drastic changes are enabled by minor adjustments to the backbone geometry including bond lengths and angles. Similarly, the conformational transitions observed in Ala_7 peptide are accomplished by a large change (64.4°) in the φ angle of the fourth residue; however, the entire chains are nearly perfectly superimposed before and after the torsion angle variation except for the atoms involved in ψ_4, φ_4, or ψ_3.[24] The observation of thermally elicited large-angle local torsion angle variations on the picosecond time scale is expected to have many experimental and computational implications. If the range of backbone torsion angles is as broad as is indicated here, it is likely that it would have implications for protein modeling, for solution NMR protein dynamics studies, and for fitting electron density in X-ray diffraction and other structure methods.[42] Variation and interdependence of the backbone dihedral angles[25-28] was predicted to be associated with isotropic chemical shifts,[7,43] NMR cross-relaxation,[44,45] and scalar coupling constants.[46]

We asked how fast local large-amplitude conformational fluctuations affect the chemical shifts of proteins, focusing on room temperature experimental solution shifts which reflect the average over the fluctuations. Although the empirical methods, like SHIFTX2[47] and SPARTA+,[48] can predict chemical shifts with high accuracy, leading to correlation coefficients of 0.98 (^{15}N), 0.99 (^{13}C α), and 0.96 (^{13}C′) with RMSE of 1.12, 0.44, and 0.53 ppm compared to the experimental results in 61 proteins,[47] their usage can be limited to frequently observed and thermally averaged conformations and so might be ill suited to sampling thermal excursions during dynamics.[49] Fragment density functional theory calculation of NMR chemical shifts for protein, on the one hand, has become increasingly practical in terms of computational time[21] and, on the other hand, can capture nuanced variations in the structure including rare events and provide accurate and physics-based predictions. The chemical prediction of GB3 using the AF-QM/MM resulted in mean unsigned errors (MUE) of 4.8 ppm with R^2 of 0.71 for ^{15}N and 2.1 ppm with R^2 of 0.79 for ^{13}C α.[50] Polenova's group compared the QM/MM calculated chemical

shifts of galection-3C with its MAS NMR chemical shifts.[51] The correlation coefficient comparing predicted vs observed shifts for $^{13}C\ \alpha$ and ^{15}N was 0.83 and 0.68 using an X-ray structure determined at 100 K; a structure determined at 293 K gives a similar correlation, which is 0.84 for $^{13}C\ \alpha$ and 0.65 for ^{15}N. Moreover, the explicit solvent molecules in QM/MM allow the interaction between the solvent and the protein to be calculated.[52-54] An explicit–implicit solvation model with only one explicit water molecule per amine and amide proton is sufficient to yield accurate results for ^{1}H (MAD ~ 0.3 ppm) and for ^{13}C (MAD ~ 3 ppm).[55] Here, we conclude that it is possible to simulate the distribution in chemical shifts at room temperature and at low temperatures using QM/MM calculations, assuming that the following technical details and procedures are followed: (1) Averaging the QM/MM calculated shifts over a long enough MD trajectory to obtain better prediction at room temperature. (2) Applying restricted minimization on room temperature MD snapshots before QM/MM to mimic the freezing out protein conformation distribution. Conformational averaging has been observed to be necessary for QM/MM prediction.[52,53,56] Previously, QM/MM prediction of a 32-amino-acid-long polypeptide averaging 500 snapshots from a 5 ns explicit solvent MD simulation gives MUE of 14.6 ppm with R^2 value of 0.81 for ^{15}N and MUE of 5.2 ppm with R^2 value of 0.99 for ^{13}C (not only $^{13}C\ \alpha$). With our procedure, we obtained a correlation for $^{13}C\ \alpha$ ($r = 0.94$) and ^{15}N ($r = 0.73$) atoms and RMSE of 4.8, 1.7, and 2.3 ppm for ^{15}N, $^{13}C\ \alpha$, and $^{13}C'$, respectively, which is significantly improved relative to the single conformation case where $^{13}C\ \alpha$ ($r = 0.78$) and ^{15}N ($r = 0.69$) are comparable to previous reports. Thus, we conclude that, while more work remains to be done, conformational averaging improves predictions of solution shifts significantly.

We asked how the fluctuations in the chemical shift might affect low temperature NMR measurements. Combining the results of QM/MM calculated shifts with the snapshots from the MD simulation, we noticed that the ^{15}N chemical shifts of protein exhibit a broad range. The variation can have a number of structural origins. The contribution of the backbone[7,57,58] and side chain[2,30,59] torsion angles to ^{15}N isotropic chemical shifts has been previously discussed; thus, their effects were carefully considered for a more accurate chemical shift prediction. Previous work indicates that high solvent accessibility correlates with high line widths in low temperature DNP-enhanced NMR spectra. As indicated in the previous literature,[60] and from the QM/MM predictions reported here, the contribution of the hydrogen bonds to both ^{15}N and ^{13}C chemical shift tensors is large and the effect of isotropic shifts can be up to 8 ppm to ^{15}N chemical shifts in model systems and smaller for ^{13}C isotropic shifts (<2 ppm for $^{13}C'$ and <0.5 for $^{13}C\ \alpha$). For ^{15}N chemical shift tensors with the hydrogen bond, δ_{11} appears to be sensitive to the presence of hydrogen bonding interactions due to its unique orientation in the molecular frame.[32] For the ^{13}C chemical shift, the tensor components depend strongly on the hydrogen-bond length and angle, particularly δ_{22}.[61] These effects may explain the empirical trends regarding solvent accessibility, and including solvent interactions in chemical shift calculation, especially anisotropy prediction, is expected to be important.[30,34,62] Accordingly, we chose to retain water molecule locations from MD simulations and to apply restricted minimization of the MD snapshots, to simulate the effects of sample freezing and predict inhomogeneous

conformational distributions and inhomogeneous chemical shift distributions in the frozen protein.

The research reported here supports the hypothesis that much of the variation in chemical shifts and broad NMR line widths for frozen samples is due to local conformational variation, where various backbone conformers are frozen into an inhomogeneous distribution at 105 K (with interconversions on a time scale slower than milliseconds).[14-18] By contrast, they are averaged into a homogeneous distribution at room temperature (with interconversions on the subnano-second time scale). This conclusion agrees well with low temperature experimental measurements of distributions in backbone ψ and correlations to the chemical shifts in various members for the ensemble. Backbone torsion angles, specifically correlated changes in ψ_i and φ_{i+1} and a resulting motion of the amide plane, are associated with these changes in NMR chemical shifts. While other structural degrees of freedom are likely to be variable and important as well, we showed here that for the N isotropic shift, ψ is a significant cause of variation.

4. CONCLUSIONS

We explored the connection between dynamics predicted by MD and NMR observables and presented strong indications of elevated thermal motions of the backbone of proteins. For liquid samples, averaging the QM/MM shift prediction over the trajectory improves the chemical shift prediction accuracy compared to predictions based on single global minimum conformations. The distributions in predicted values also agree well with the breadth of low temperature NMR spectra. Variation in the backbone torsion angles, ψ specifically, appears to have marked effects on the ^{15}N isotropic shifts.

Supplementary Material

Refer to Web version on PubMed Central for supplementary material.

ACKNOWLEDGMENTS

This work was supported by a grant from the NSF (MCB 1913885) and a Biomedical Technology Development and Dissemination Center grant from the NIH (1RM1GM145397-01). We thank David Case and Yunyao Xu for helpful discussions.

Biographies

Xu Yi obtained a Bachelor of Science degree from Nanjing University in 2017, followed by a Ph.D. in Chemistry from Columbia University in 2022 under the supervision of Professor Ann E. McDermott. Currently, she is engaged in the field of laboratory virtualization for chemistry and biotechnology while concurrently pursuing a degree in Computer Science at the University of Illinois Urbana–Champaign.

Lichirui Zhang earned his B.S. in Chemistry from Nankai University in 2017 and a Ph.D. from Columbia University in 2023, mentored by Prof. Richard A. Friesner. He is currently a Senior Scientist at Schrödinger Inc., focusing on the development of deep learning and physics-based computational methods for modeling biomolecules.

Richard A. Friesner was born in New York, NY, in 1952. He received his BS degree in chemistry from the University of Chicago in 1973. He obtained his Ph.D. in 1979 at the University of California, Berkeley, working in the laboratory of Kenneth Sauer. He then spent three years as a postdoctoral fellow working with Robert Silbey at the Massachusetts Institute of Technology. He joined the Chemistry Department at the University of Texas at Austin in 1982 as an Assistant Professor. In 1990, he became Professor of Chemistry at Columbia University. His work is currently focused on computational modeling of complex systems biology and materials sciences. Specific interests include protein structure prediction, structure based drug design, modeling of enzyme reactions, and modeling of nanosystems such as silicon nanoparticles and carbon nanotubes with a particular focus on solar energy applications.

Ann E. McDermott obtained her Bachelor of Science in Chemistry from Harvey Mudd College in Claremont, CA, in 1981. In 1988, she obtained her doctoral degree at U.C. Berkeley in the Department of Chemistry with Kenneth Sauer and Melvin Klein. As a postdoctoral researcher she worked with Robert G Griffin at The Massachusetts Institute of Technology. She joined Columbia University as a Professor in Chemistry Department in 1991. Her research exploits Nuclear Magnetic Resonance to study the functions, structures, and dynamics of proteins including enzymes, viral proteins, membrane proteins and amyloid proteins.

REFERENCES

(1). De Dios AC; Pearson JG; Oldfield E Secondary and Tertiary Structural Effects on Protein NMR Chemical Shifts: An Ab Initio Approach. Science (1979) 1993, 260 (5113), 1491–1496.

(2). Oldfield E. Chemical Shifts in Amino Acids, Peptides, and Proteins: From Quantum Chemistry to Drug Design. Annu. Rev. Phys. Chem 2002, 53 (2), 349–378. [PubMed: 11972012]

(3). Case DA Using Quantum Chemistry to Estimate Chemical Shifts in Biomolecules. Biophys. Chem 2020, 267 (September), 106476. [PubMed: 33035752]

(4). Wishart DS; Sykes BD; Richards FM Relationship between Nuclear Magnetic Resonance Chemical Shift and Protein Secondary Structure. J. Mol. Biol 1991, 222 (2), 311–333. [PubMed: 1960729]

(5). Wang Y. Probability-Based Protein Secondary Structure Identification Using Combined NMR Chemical-Shift Data. Protein Sci. 2002, 11 (4), 852–861. [PubMed: 11910028]

(6). Wang Y; Jardetzky O Predicting 15N Chemical Shifts in Proteins Using the Preceding Residue-Specific Individual Shielding Surfaces from φ, Ψi-1, and X1 Torsion Angles. J. Biomol. NMR 2004, 28 (4), 327–340. [PubMed: 14872125]

(7). Le H; Oldfield E Correlation between 15N NMR Chemical Shifts in Proteins and Secondary Structure. J. Biomol. NMR 1994, 4 (3), 341–348. [PubMed: 8019141]

(8). Li DW; Hansen AL; Yuan C; Bruschweiler-Li L; Bruschweiler R DEEP Picker Is a Deep Neural Network for Accurate Deconvolution of Complex Two-Dimensional NMR Spectra. Nat. Commun 2021, 12 (1), 5229. [PubMed: 34471142]

(9). Robustelli P; Stafford KA; Palmer AG Interpreting Protein Structural Dynamics from NMR Chemical Shifts. J. Am. Chem. Soc 2012, 134 (14), 6365–6374. [PubMed: 22381384]

(10). Pérez-Conesa S; Keeler EG; Zhang D; Delemotte L; McDermott AE Informing NMR Experiments with Molecular Dynamics Simulations to Characterize the Dominant Activated State of the KcsA Ion Channel. J. Chem. Phys 2021, 154 (16), 165102. [PubMed: 33940802]

(11). Kraus J; Gupta R; Lu M; Gronenborn AM; Akke M; Polenova T Accurate Backbone 13C and 15N Chemical Shift Tensors in Galectin-3 Determined by MAS NMR and QM/MM: Details

of Structure and Environment Matter. ChemPhysChem 2020, 21 (13), 1436–1443. [PubMed: 32363727]

(12). Sergeyev IV; Itin B; Rogawski R; Day LA; McDermott AE Efficient Assignment and NMR Analysis of an Intact Virus Using Sequential Side-Chain Correlations and DNP Sensitization. Proc. Natl. Acad. Sci. U.S.A 2017, 114 (20), 5171–5176. [PubMed: 28461483]

(13). Bajaj VS; van der Wel PCA; Griffin RG Observation of a Low-Temperature, Dynamically Driven Structural Transition in a Polypeptide by Solid-State NMR Spectroscopy. J. Am. Chem. Soc 2009, 131 (1), 118–128. [PubMed: 19067520]

(14). Su Y; Hong M Conformational Disorder of Membrane Peptides Investigated from Solid-State NMR Line Widths and Line Shapes. J. Phys. Chem. B 2011, 115 (36), 10758–10767. [PubMed: 21806038]

(15). Gupta R; Zhang H; Lu M; Hou G; Caporini M; Rosay M; Maas W; Struppe J; Ahn J; Byeon IJL; et al. Dynamic Nuclear Polarization Magic-Angle Spinning Nuclear Magnetic Resonance Combined with Molecular Dynamics Simulations Permits Detection of Order and Disorder in Viral Assemblies. J. Phys. Chem. B 2019, 123 (24), 5048–5058. [PubMed: 31125232]

(16). Bayro MJ; Debelouchina GT; Eddy MT; Birkett NR; MacPhee CE; Rosay M; Maas WE; Dobson CM; Griffin RG Intermolecular Structure Determination of Amyloid Fibrils with Magic-Angle Spinning and Dynamic Nuclear Polarization NMR. J. Am. Chem. Soc 2011, 133 (35), 13967–13974. [PubMed: 21774549]

(17). Reggie L; Lopez JJ; Collinson I; Glaubitz C; Lorch M Dynamic Nuclear Polarization-Enhanced Solid-State NMR of a 13C-Labeled Signal Peptide Bound to Lipid-Reconstituted Sec Translocon. J. Am. Chem. Soc 2011, 133 (47), 19084–19086. [PubMed: 22040139]

(18). Lopez Del Amo JM; Schneider D; Loquet A; Lange A; Reif B Cryogenic Solid State NMR Studies of Fibrils of the Alzheimer's Disease Amyloid-β Peptide: Perspectives for DNP. J. Biomol. NMR 2013, 56 (4), 359–363. [PubMed: 23793606]

(19). Yi X. Solid-State NMR Lineshape Broadening at Cryogenic Temperatures. Ph.D. Thesis, Columbia University, 2023.

(20). He X; Wang B; Merz KM Protein NMR Chemical Shift Calculations Based on the Automated Fragmentation QM/MM Approach. J. Phys. Chem. B 2009, 113 (30), 10380–10388. [PubMed: 19575540]

(21). Swails J; Zhu T; He X; Case DA AFNMR: Automated Fragmentation Quantum Mechanical Calculation of NMR Chemical Shifts for Biomolecules. J. Biomol. NMR 2015, 63 (2), 125–139. [PubMed: 26232926]

(22). Rogawski R. Dynamic Nuclear Polarization with Biradical Affinity Reagents. Ph.D. Thesis, Columbia University, 2018. DOI: 10.7916/D8ZG802G.

(23). Sawaya MR; Kraut J Loop and Subdomain Movements in the Mechanism of Escherichia Coli Dihydrofolate Reductase: Crystallographic Evidence. Biochemistry 1997, 36 (3), 586–603. [PubMed: 9012674]

(24). Fitzgerald JE; Jha AK; Sosnick TR; Freed KF Polypeptide Motions Are Dominated by Peptide Group Oscillations Resulting from Dihedral Angle Correlations between Nearest Neighbors. Biochemistry 2007, 46 (3), 669–682. [PubMed: 17223689]

(25). Go M; Go N Fluctuations of an α-Helix. Biopolymers 1976, 15 (6), 1119–1127. [PubMed: 1268317]

(26). Wasserman ZR; Salemme FR A Molecular Dynamics Investigation of the Elastomeric Restoring Force in Elastin. Biopolymers 1990, 29 (12–13), 1613–1631. [PubMed: 2386809]

(27). García AE Large-Amplitude Nonlinear Motions in Proteins. Phys. Rev. Lett 1992, 68 (17), 2696–2699. [PubMed: 10045464]

(28). Karplus M; McCammon JA; Gelin BR Dynamics of Folded Proteins. Nature 1977, 267 (June), 585–590. [PubMed: 301613]

(29). Yi X; Fritzsching KJ; Rogawski R; Xu Y; Mcdermott AE Contribution of Protein Conformational Heterogeneity to NMR Lineshapes at Cryogenic Temperatures. bioRxiv 2023, DOI: 10.1101/2023.01.24.525358.

(30). Cai L; Fushman D; Kosov DS Density Functional Calculations of 15N Chemical Shifts in Solvated Dipeptides. J. Biomol NMR 2008, 41 (2), 77–88. [PubMed: 18484179]

(31). Xu XP; Case DA Probing Multiple Effects on 15N, 13Cα, 13Cβ, and 13C′ Chemical Shifts in Peptides Using Density Functional Theory. Biopolymers 2002, 65 (6), 408–423. [PubMed: 12434429]

(32). Paramasivam S; Gronenborn AM; Polenova T Backbone Amide 15N Chemical Shift Tensors Report on Hydrogen Bonding Interactions in Proteins: A Magic Angle Spinning NMR Study. Solid State Nucl. Magn. Reson 2018, 92 (March), 1–6. [PubMed: 29579703]

(33). Takeda N; Kuroki S; Kurosu H; Ando L 13C-NMR Chemical Shift Tensor and Hydrogen Bonded Structure of Glycine Containing Peptides in a Single Crystal. Biopolymers 1999, 50 (1), 61–69.

(34). Takegoshi K; Naito A; McDowell CA Intermolecular Hydrogen-Bonding Effects on the 13C NMR Shielding Tensor of the Carbonyl Carbon Nucleus in a Single Crystal of Dimedone. J. Magn. Res. (1969) 1985, 65 (1), 34–42.

(35). Xu Y; Havenith M Perspective: Watching Low-Frequency Vibrations of Water in Biomolecular Recognition by THz Spectroscopy. J. Chem. Phys 2015, 143, 170901. [PubMed: 26547148]

(36). Henzler-Wildman KA; Lei M; Thai V; Kerns SJ; Karplus M; Kern D A Hierarchy of Timescales in Protein Dynamics Is Linked to Enzyme Catalysis. Nature 2007, 450 (7171), 913–916. [PubMed: 18026087]

(37). Mu Y; Nguyen PH; Stock G Energy Landscape of a Small Peptide Revealed by Dihedral Angle Principal Component Analysis. Prot. Struct. Funct. Genet 2005, 58 (1), 45–52.

(38). Gupta AK; Natarajan U Tacticity Effects on Conformational Structure and Hydration of Poly-(Methacrylic Acid) in Aqueous Solutions-a Molecular Dynamics Simulation Study. Mol. Simul 2016, 42 (9), 725–736.

(39). Ravikumar A; Srinivasan N Hypervariability of Accessible and Inaccessible Conformational Space of Proteins. Curr. Res. Struct. Biol 2021, 3 (June), 229–238. [PubMed: 34604793]

(40). Grassein P; Delarue P; Nicolaï A; Neiers F; Scheraga HA; Maisuradze GG; Senet P; Senet P Curvature and Torsion of Protein Main Chain as Local Order Parameters of Protein Unfolding. J. Phys. Chem. B 2020, 124 (22), 4391–4398. [PubMed: 32392067]

(41). Ravikumar A; Srinivasan N Hypervariability of Accessible and Inaccessible Conformational Space of Proteins. Curr. Res. Struct. Biol 2021, 3 (June), 229–238. [PubMed: 34604793]

(42). Keedy DA; Van Den Bedem H; Sivak DA; Petsko GA; Ringe D; Wilson MA; Fraser JS Crystal Cryocooling Distorts Conformational Heterogeneity in a Model Michaelis Complex of DHFR. Structure 2014, 22 (6), 899–910. [PubMed: 24882744]

(43). Le H; Oldfield E Ab Initio Studies of Amide-15N Chemical Shifts in Dipeptides: Applications to Protein NMR Spectroscopy. J. Phys. Chem 1996, 100 (40), 16423–16428.

(44). Williams JC; McDermott AE Variable NMR Spin-Lattice Relaxation Times in Secondary Amides: Effect of Ramachandran Angles on Librational Dynamics. J. Phys. Chem. B 1998, 102 (32), 6248–6259.

(45). Déméné H; Sugàr IP Protein Conformation and Dynamics. Effects of Crankshaft Motions on 1 H NMR Cross-Relaxation Effects. J. Phys. Chem. A 1999, 103 (24), 4664–4672.

(46). Shen Y; Roche J; Grishaev A; Bax A Prediction of Nearest Neighbor Effects on Backbone Torsion Angles and NMR Scalar Coupling Constants in Disordered Proteins. Protein Sci. 2018, 27 (1), 146–158. [PubMed: 28884933]

(47). Han B; Liu Y; Ginzinger SW; Wishart DS SHIFTX2: Significantly Improved Protein Chemical Shift Prediction. J. Biomol. NMR 2011, 50 (1), 43–57. [PubMed: 21448735]

(48). Shen Y; Bax A SPARTA+: A Modest Improvement in Empirical NMR Chemical Shift Prediction by Means of an Artificial Neural Network. J. Biomol. NMR 2010, 48 (1), 13–22. [PubMed: 20628786]

(49). Sumowski CV; Hanni M; Schweizer S; Ochsenfeld C Sensitivity of Ab Initio vs Empirical Methods in Computing Structural Effects on NMR Chemical Shifts for the Example of Peptides. J. Chem. Theory Comput 2014, 10 (1), 122–133. [PubMed: 26579896]

(50). Zhu T; He X; Zhang JZH Fragment Density Functional Theory Calculation of NMR Chemical Shifts for Proteins with Implicit Solvation. Phys. Chem. Chem. Phys 2012, 14 (21), 7837–7845. [PubMed: 22314755]

(51). Kraus J; Gupta R; Yehl J; Lu M; Case DA; Gronenborn AM; Akke M; Polenova T Chemical Shifts of the Carbohydrate Binding Domain of Galectin-3 from Magic Angle Spinning NMR

and Hybrid Quantum Mechanics/Molecular Mechanics Calculations. J. Phys. Chem. B 2018, 122 (11), 2931–2939. [PubMed: 29498857]

(52). Exner TE; Frank A; Onila I; Möller HM Toward the Quantum Chemical Calculation of NMR Chemical Shifts of Proteins. 3. Conformational Sampling and Explicit Solvents Model. J. Chem. Theory Comput 2012, 8 (11), 4818–4827. [PubMed: 26605634]

(53). Dračínský M; Möller HM; Exner TE Conformational Sampling by Ab Initio Molecular Dynamics Simulations Improves NMR Chemical Shift Predictions. J. Chem. Theory Comput 2013, 9 (8), 3806–3815. [PubMed: 26584127]

(54). Chandy SK; Thapa B; Raghavachari K Accurate and Cost-Effective NMR Chemical Shift Predictions for Proteins Using a Molecules-in-Molecules Fragmentation-Based Method. Phys. Chem. Chem. Phys 2020, 22 (47), 27781–27799. [PubMed: 33244526]

(55). Chandy SK; Thapa B; Raghavachari K Accurate and Cost-Effective NMR Chemical Shift Predictions for Proteins Using a Molecules-in-Molecules Fragmentation-Based Method. Phys. Chem. Chem. Phys 2020, 22 (47), 27781–27799. [PubMed: 33244526]

(56). Case DA Using Quantum Chemistry to Estimate Chemical Shifts in Biomolecules. Biophys. Chem 2020, 267 (August), 106476. [PubMed: 33035752]

(57). Luman NR; King MP; Augspurger JD Predicting15N Amide Chemical Shifts in Proteins. I. An Additive Model for the Backbone Contribution. J. Comput. Chem 2001, 22 (3), 366–372.

(58). Wang L; Markley JL Empirical Correlation between Protein Backbone 15N and 13C Secondary Chemical Shifts and Its Application to Nitrogen Chemical Shift Re-Referencing. J. Biomol. NMR 2009, 44 (2), 95–99. [PubMed: 19436955]

(59). Xu XP; Case DA Automated Prediction of 15N, 13Cα, 13Cβ and 13C′ Chemical Shifts in Proteins Using a Density Functional Database. J. Biomol. NMR 2001, 21 (4), 321–333. [PubMed: 11824752]

(60). Xu XP; Case DA Probing Multiple Effects on 15N, 13Cα, 13Cβ, and 13C′ Chemical Shifts in Peptides Using Density Functional Theory. Biopolymers 2002, 65 (6), 408–423. [PubMed: 12434429]

(61). Takeda N; Kuroki S; Kurosu H; Ando I; Ando L 13C-NMR Chemical Shift Tensor and Hydrogen-Bonded Structure of Glycine-Containing Peptides in a Single Crystal. Biopolymers 1999, 50 (1), 61–69.

(62). La Penna G; Mori Y; Kitahara R; Akasaka K; Okamoto Y Modeling 15N NMR Chemical Shift Changes in Protein Backbone with Pressure. J. Chem. Phys 2016, 145 (8), 085104. [PubMed: 27586953]

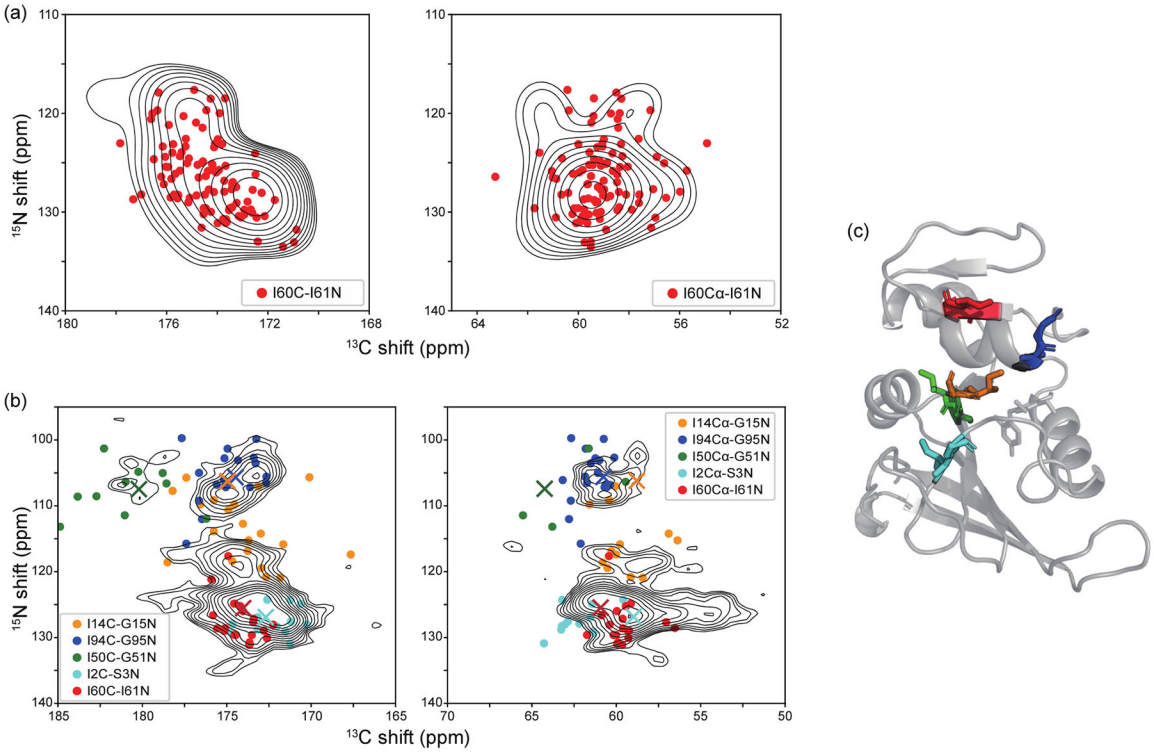

Figure 1.

Low temperature solid-state NMR (SSNMR) ^{15}N—^{13}C correlation spectra of (a) ^{13}C,^{15}N-Ile labeled *E. coli* DHFR:TMP (I-DHFR) and (b) ^{13}C,^{15}N-Ile, ^{15}N-Gly labeled *E. coli* DHFR:TMP (IG-DHFR) measured using DNP enhanced SSNMR at 105 K. Ile60-Ile61(sheet) is the only residue pair expected in I-DHFR DNP spectra because of a sparse isotopic enrichment scheme (Ile only is enriched). In IG-DHFR, 4 more residue pairs are observed (Ile2-Ser3 (sheet), Ile14-Gly15 (coil), Ile50-Gly51 (helix), Ile94-Gly95 (coil)). The 5 pairs are highlighted with stick rendering of the side chains in cartoon of the structure of *E. coli* DHFR:TMP (c): I2-S3 (green), I14-G15 (cyan), I50-G51 (blue), I94-G95 (orange), and I60-I61 (red). The predicted chemical shifts for conformations sampled from MD and predicted with QM/MM are overlaid: 100 snapshots were minimized and calculated for Ile60-Ile61 in (a) and 20 snapshots were used for residue pairs in (b). Both C and N chemical shifts from QM/MM calculation were calibrated with the offsets from average chemical shifts of snapshots and solution-state NMR chemical shifts. The lowest contour levels in SSNMR spectra are set to be 15 times (a) and 3.5 times (b) the RMS noise level, and the multiplier is 1.3 for both (a) and (b). The peak at $^{13}C\alpha$ 53–55 ppm in (b) results from a spinning sideband and was not predicted. The cross markers in (b) indicate the solution-state NMR chemical shifts for the 5 residue pairs.

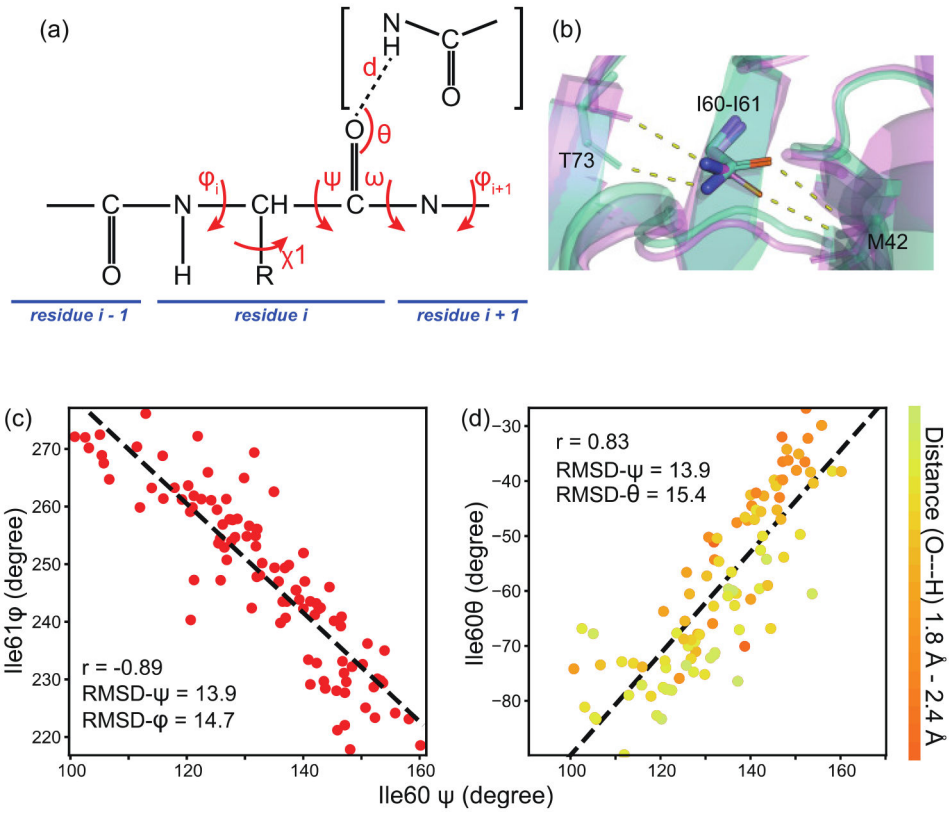

Figure 2.

Protein structural variation during MD simulation at 300 K. (a) Dihedral angles and H bond angle/distance were analyzed. (b) Structure overlay of Ile60-Ile61 in snapshots at 200 ns in MD with Ile60 ψ = 160° (green) and at 160 ns in MD with Ile60 ψ = 113° (pink) indicates that the Cα position is unchanged while the N (blue) and carbonyl O (orange) move. (c) There is strong correlation between Ile61 φ and Ile60 ψ. Each scatter point represents one snapshot from MD simulation extracted every 10 ns. The correlation coefficient is −0.89. (d) The correlation plot of Ile60 θ and Ile60 ψ shows strong correlation between backbone torsion angle and H bond angle. The H bond angle θ is defined as the angle between the H bond (O---H) and C═O. Ile60 is located in a β-sheet structure, and its O forms a H bond with Met42 ^{N}H in MD simulation. The closest water molecule is ~7.5 Å away from the Ile60 O during the trajectory. The correlation between ψ_{i+1}, φ_i, and H bond angle θ_i is not unique for I60-I61, as shown in Figure S7.

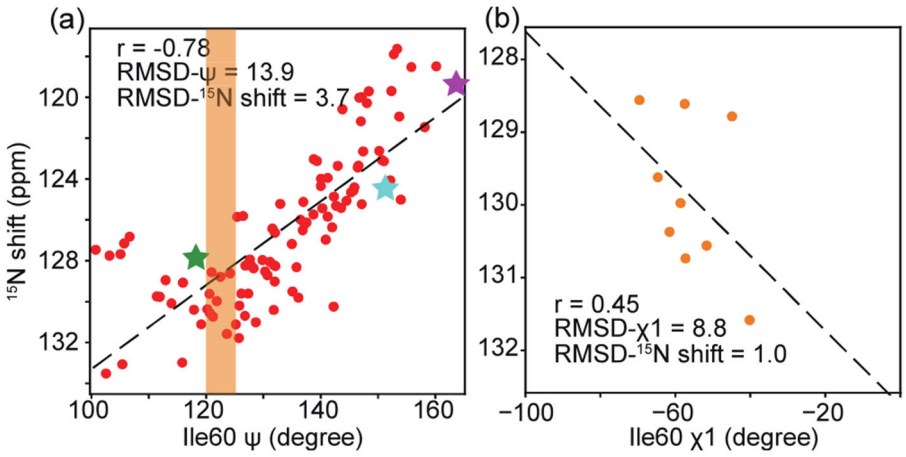

Figure 3.

(a) QM/MM calculated Ile61N isotropic shifts are plotted as a function of I60 ψ from 100 minimized snapshots from the MD trajectory (red, circle). Three ψ values were measured experimentally at three ^{15}N shift positions for Ile60 in low temperature DNP-enhanced NMR experiments[19] and are shown here depicted with stars. The correlation between ψ angles and chemical shifts from both prior experimental and these computational results match well. The side chain torsion angle I60 χ1 was plotted with ^{15}N shifts for snapshots with similar backbone torsion angle ψ, 120° < I60 ψ < 125° (b). Ile61N shifts vary up to 5 ppm with a 5° range of I60 ψ, and I60 χ1 is likely to contribute to this variation.

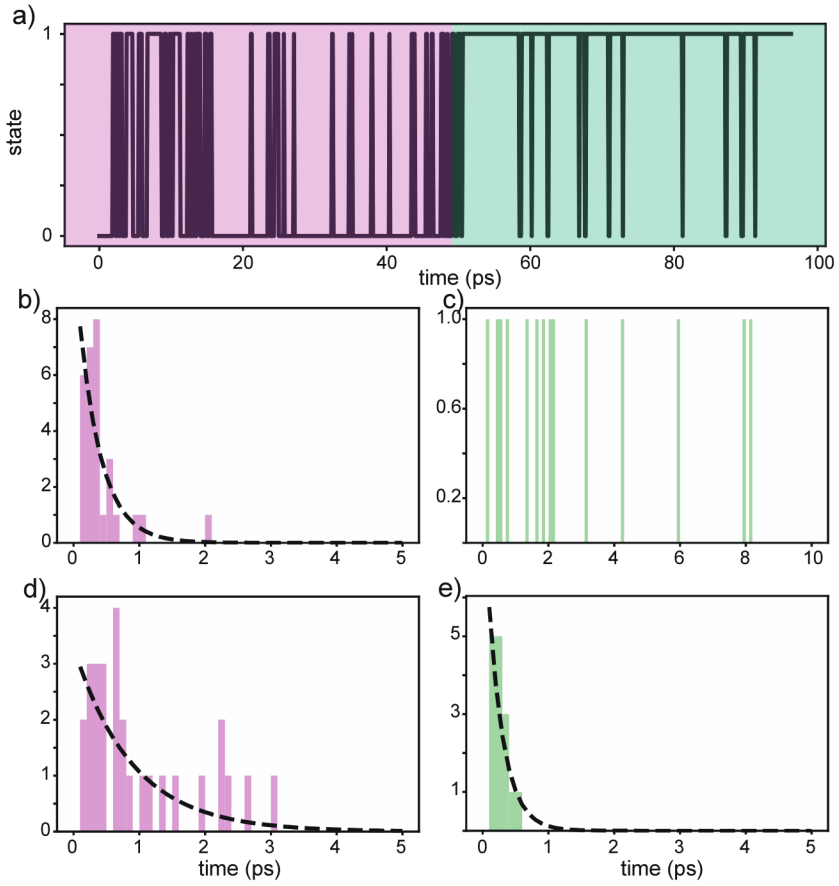

Figure 4.

(a) Two states were defined based on Ile60 ψ variation (Figure S16a) in 100 ps MD simulation, State 0 (Figure S16b) with Ile60 ψ < 125° and State 1 (Figure S16c) with Ile60 ψ > 125°. State 0 is more dominant before (pink) 50 ps and State 1 after (green) 50 ps. The histograms of the residence times for Ile60 ψ staying in State 0 (d, e) or State 1 (b, c) before (b, d, pink) and after (c, e green) 50 ps were fit with a single exponential function (black dash line). For the first 50 ps trajectory, the residence time is 0.89 ± 0.18 ps for State 0 and 0.34 ± 0.05 ps for State 1. After 50 ps, the residence time is 0.23 ± 0.02 ps for State 0. The residence time for State 1 is longer than what can be identified through this trajecotry.